Determination of cross sections for the ^{80}Kr(n, 2n)^{79}Kr reaction in the neutron energy range of 13−15 MeV*

Junhua Luo (罗均华)[1,2†] Long He (贺龙)[2] Liang Zhou (周亮)[3] Li Jiang (蒋励)[4]

[1]Department of Basic Science, Lanzhou Institute of Technology, Lanzhou 730050, China
[2]Institute of New Energy, Hexi University, Zhangye 734000, China
[3]School of Physics and Electromechanical Engineering, Hexi University, Zhangye 734000, China
[4]Institute of Nuclear Physics and Chemistry, China Academy of Engineering Physics, Mianyang 621900, China

Abstract: In this study, neutron activation experiments were performed to measure the (n, 2n) reaction cross section for ^{80}Kr at five neutron energies, 13.59±0.12, 13.86±0.15, 14.13±0.16, 14.70±0.13, and 14.94±0.02 MeV, using a highly enriched gaseous sample. The neutron energies and their uncertainties were determined using the Q-value equation for the ^{3}H(d, n)^{4}He reaction, accounting for the solid angle of the sample. The ^{93}Nb(n, 2n)^{92m}Nb reaction was employed to monitor the neutron flux. Eight characteristic gamma rays of the produced nucleus were selected to determine the activity of the generated nuclei. The final cross sections were obtained using a weighted average method. The self-absorption and cascade of rays, as well as the geometry and solid angles of the sample, were corrected. The ^{80}Kr(n, 2n)^{79}Kr reaction cross sections obtained in this work exhibited the smallest uncertainty than the values in existing literature, which provided improved experimental constraints for the prediction of excitation curves, thereby enhancing the quality of the corresponding database. The measured results were compared with previously reported experimental values, empirical and systematic formula predictions, theoretical calculations from TALYS-1.96 with six adjustable energy level densities, and evaluated database results. Our experimental results demonstrated high precision and extended the energy range appropriately, offering valuable insights for future studies.

Keywords: krypton-80, activation method, (n, 2n) reaction, cross section, nuclear model calculation.

DOI: 10.1088/1674-1137/adcc90 **CSTR:** 32044.14.ChinesePhysicsC.49084005

I. INTRODUCTION

The cross sections of nuclear reactions induced by neutrons serve as crucial data for nuclear reaction modeling, nuclear technology applications, nuclear weapon verification, and nuclear medicine detection [1−5]. The International Atomic Energy Agency (IAEA) has collected various reaction cross sections, including (n, 2n), (n, p), (n, α), (n, γ), (n, $n'\alpha$), (n, d), and (n, t), through the Experimental Nuclear Reaction Data (EXFOR) database [1, 4−10]. Among these, the reaction mechanism and cross section measurements of the (n, 2n) reaction caused by fast neutrons have always been a research focus in nuclear physics owing to their importance for neutron dose measurement, deuterium-tritium fusion reactor design, and neutron shielding for accelerator facilities. Additionally, these data are essential for estimating induced radioactivity, nuclear transmutation, and material radiation damage [1, 2, 4]. In reactor physics, krypton (Kr) is a critical neutron-absorbing fission product that significantly influences neutron economy and fuel cycle management. During reactor operation, gaseous Kr isotopes are generated via fission processes. These isotopes exhibit non-negligible neutron absorption cross sections, thereby reducing neutron availability for sustaining chain reactions or breeding fissile materials [11−13]. According to the EXFOR database, the (n, 2n) reactions at a neutron energy of 14 MeV are the most widely studied for solid natural targets as they have larger cross sections than other reactions. However, for gas targets, the difficulty in creating the target has resulted in insufficient measurement of reaction cross sections, with no corresponding cross section data available to date. Regarding the experimental measurement of the cross sections for neutron-induced krypton isotope nuclear reactions, Kondaiah *et al*. [14] first measured the cross sections of ^{78}Kr(n, 2n)^{77}Kr, ^{80}Kr(n, 2n)$^{79(m+g)}$Kr, ^{80}Kr(n, 2n)^{79m}Kr, ^{82}Kr(n, 2n)^{81m}Kr, ^{86}Kr(n, 2n)^{85m}Kr, ^{80}Kr(n, p)^{80m}Br, ^{82}Kr(n, p)$^{82(m+g)}$Br, ^{84}Kr(n, p)^{84}Br, and ^{85}Kr(n, α)^{83g}Se reaction channels at a neutron energy of 14.4 MeV in 1968. These measure-

Received 11 March 2025; Accepted 15 April 2025; Published online 16 April 2025
* Supported by the National Natural Science Foundation of China (12375295, 12165006)
† E-mail: luojh71@163.com

ments were performed using a natural abundance solid-state target fabricated from powders of the inert gas quinol-clathrate, $[C_6H_4(OH)_2]_3$-0.895Kr. Recently, Zeng *et al.* [15] measured the cross section of the ^{78}Kr(n, $2n$)^{77}Kr reaction in the energy range of 13−15 MeV using a highly enriched ^{78}Kr gas target. However, neutron-induced cross sections of other krypton isotope reactions in a wide energy range have not been reported.

Systematics is an effective method for calculating the cross sections of nuclear reactions without experimental data [16−23]. The systematic formula is simplified based on the statistical model, considering Q-value dependence. The mass number (A) and asymmetric parameter ($(N-Z)/A$) of the target nuclei are important input values in the formula. A reliable systematic formula requires a large number of high-precision experimental cross section data to accurately fit the coefficients at specific neutron energy points. However, the experimental cross sections of A=80 and $(N-Z)/A$=0.1 are not included in the fitting process for the existing (n, $2n$) reaction cross section systematic formula. An alternative approach for predicting the cross section of the (n, $2n$) reaction is based on neural networks; however, it requires a large amount of experimental cross section data for training [1]. In the ^{80}Kr(n, $2n$)^{79m,g}Kr reaction, the excited state of the formed nucleus decays to the ground state via 100% isomeric transition (see Fig. 1). In 1968, the Kondaiah *et al.* [14] used a characteristic gamma ray of 398 keV to measure

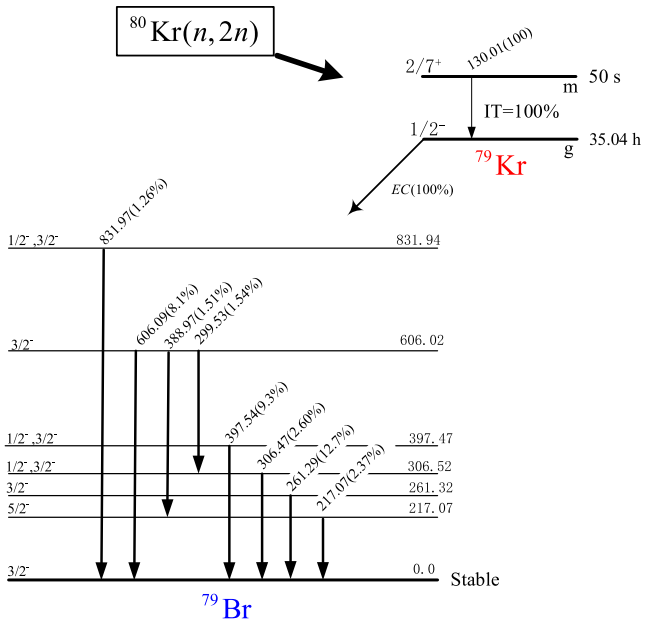

Fig. 1. (color online) Metastable and ground states involved in the ^{80}Kr(n, $2n$)^{79m,g}Kr reactions [24]. All energy values are in kiloelectronvolts. The bold black line indicates the transitions originating from both the excited and ground states, whereas the intensities listed in parentheses correspond to the rays emitted from these two states.

the cross section of the ^{80}Kr(n, $2n$)^{79}Kr reaction at a neutron energy of 14.4±0.3 MeV. They reported a cross section value of 810 mb with an uncertainty of 7.4% based on a half-life of 34.92 h and ray intensity of 7.7%. The latest results for these two data are 35.04 h and 9.3%, respectively [24].

In this study, the latest decay data were used to determine the cross section of the ^{80}Kr(n, $2n$)^{79}Kr reaction. Highly enriched ^{80}Kr isotope gas samples were employed to eliminate the influence of neighboring isotope ^{78}Kr on the target reaction through (n, γ) reactions. We selected eight characteristic gamma rays to measure the activity of the generated nuclei, and the corresponding results were averaged with appropriate weighting to minimize the uncertainty in the measured cross section. Finally, we compared the final results with the experimental values reported in earlier literature [14], TALYS theoretical calculation curves [25], and evaluation curves of databases ENDF/B-VIII.0 [26], BROND-3.1 [27], JEFF- 3.3 [28], JENDL-5 [29], and TENDL-2023 [30].

II. EXPERIMENTAL PROCESS

A. Target material

Kr is an inert, environmentally friendly, and noncorrosive gas at ambient temperature and pressure. It has six stable isotopes, with natural abundance as follows: ^{78}Kr (0.355%), ^{80}Kr (2.286%), ^{82}Kr (11.593%), ^{83}Kr (11.500%), ^{84}Kr (56.987%), and ^{86}Kr (17.279%) [31]. To increase the number of atomic nuclei in the sample target while minimizing the influence of adjacent isotopes on the target reaction, we used the highly enriched (99.928%) ^{80}Kr isotope gas. The highly enriched ^{80}Kr gas was provided by ISOFLEX USA. The other isotopes and abundances in the gas included ^{78}Kr (0.0488%), ^{82}Kr (0.0016%), ^{83}Kr (0.004%), ^{84}Kr (0.004%), and ^{86}Kr (0.004%). The gas was stored in a stainless steel container shaped like a sphere, with an inner diameter of 20.0 mm and a wall thickness of 1.0 mm, where the pressure exceeded 100 atmospheres. Background measurements were conducted on the stainless steel materials used to manufacture the spherical containers. The gas was filled with liquid nitrogen and sealed after being weighed five times over a period of 76 days, with a weight change rate of less than 0.16%. A photograph of the spherical samples is presented in Fig. 2. After gamma ray spectrum measurements, the weight of the gas was obtained by subtracting the container's weight from the total weight. The weight of the ^{80}Kr gas used in this experiment was 0.18−0.29 g.

B. Neutron sources and irradiation

The neutron irradiation experiment was performed on the K-400 neutron generator at the China Academy of

Fig. 2. (color online) Photograph of the high-pressure spheres used in this work.

Engineering Physics (CAEP). The sample, composed of ZrNbAl-^{80}Kr-AlNbZr, was coated with a cadmium sheet (1.0 mm thick and 99.95% pure) to minimize the influence of low-energy neutrons. Zr, Nb, and Al were metal circular discs with diameters of 20 mm; their purities were 99.5%, 99.99%, and 99.99% and thicknesses were 0.3, 0.4, and 0.3 mm, respectively. The sample groups were fixed at angles of 0º, 45º, 90º, 110º, and 135º relative to the deuterium beam incidence, with the sample placed 50 mm from the center of the T-Ti target (see Fig. 3). The ^{3}H(d, n)^{4}He reaction produced monoenergetic neutrons with energies of 13−15 MeV, whereas the average energy of the incident deuterium beam was 135 keV, with a beam intensity of 240 μA. The neutron yield was approximately (4−5)×10^{10} n/s. The sample group was irradiated continuously for 2 h. α-Particle counts were measured using a Au-Si surface barrier detector positioned at 135° to compensate for fluctuations in the neutron flux.

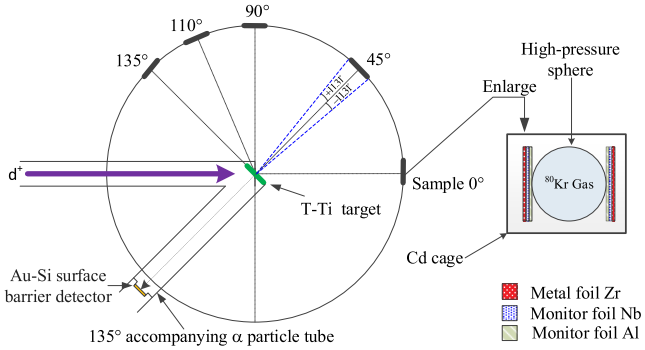

Fig. 3. (color online) Schematic of the relative position of T-Ti target and ^{80}Kr sample.

C. Determination of neutron energy

The neutron energy at the location of the irradiated sample was calculated using the Q-value equation of the ^{3}H(d, n)^{4}He reaction [32]. The neutron energies at 135°, 110°, 90°, 45°, and 0° were 13.59±0.12, 13.86±0.15, 14.13±0.16, 14.70±0.13, and 14.94±0.02 MeV, respectively. The uncertainty incorporated both the distance from the sample to the T-Ti target and the solid angle corresponding to the sample size. The results obtained using the cross section ratio method for ^{90}Zr(n, 2n)$^{89m+g}$Zr and ^{93}Nb(n, 2n)^{92m}Nb reactions [33], along with the neutron energy method for D-T reactions on a large sample provided earlier [34], are consistent with the above results within the range of uncertainty.

D. Scale of detector efficiency

In general, the efficiency of a high-purity germanium detector (HPGe) depends on the incident photon energy (E_γ). Accurately determining the detector efficiency in the gamma ray energy range below 80 keV is difficult. Before measuring the gamma ray spectrum of irradiated samples, the efficiency of the HPGe detector was calibrated using four standard sources (^{152}Eu, ^{133}Ba, ^{137}Cs, and ^{226}Ra). The fitting spline function, $\varepsilon(E_\gamma) = \sum_{n=0}^{5} B_n [\ln(E_\gamma)]^n$ [8], with a correlation coefficient (R^2) of 0.9988, was used to obtain gamma ray efficiency. The fitting results are shown in Fig. 4. The Monte Carlo method was applied to correct the geometric differences between the spherical sample and standard source.

E. Gamma spectroscopic measurements

After neutron irradiation, the ^{80}Kr gas sample was measured multiple times using an HPGe detector (GEM-60P). The Zr, Nb, and Al sheets positioned at the front and back of the sample were measured independently

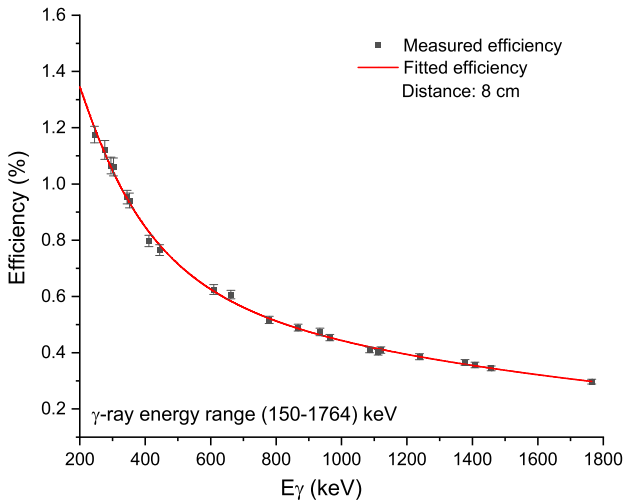

Fig. 4. (color online) Standard source calibration point and efficiency fitting curve.

from the gas sample. The HPGe detector has an energy resolution of 1.69 keV for the 1.332 MeV gamma ray of ^{60}Co and a relative efficiency of approximately 68%. A typical gamma ray spectrum obtained through the data acquisition system (ORTEC® (GammaVision®)) [35] is shown in Fig. 5. This spectrum was measured after a 21.7 h cooling period, with a measurement time of 23.5 min. The main characteristic rays of the sample are labeled in the figure. The blue text marks the line from the container (320.08 keV from ^{54}Fe(n, α)^{51}Cr ($T_{1/2}$ = 27.7025 d), 834.48 keV from ^{54}Fe(n, p)^{54}Mn ($T_{1/2}$ = 312.20 d), and 846.76 keV from ^{56}Fe(n, p)^{56}Mn ($T_{1/2}$ = 2.5789 h)) [31]. Table 1 provides an overview of the reactions and the radioactive decay properties of the corresponding reaction products.

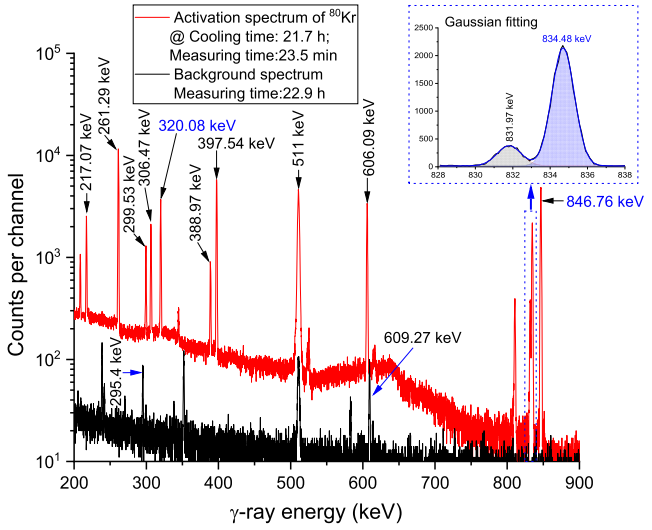

Fig. 5. (color online) Gamma ray spectrum of krypton recorded approximately 21.7 h after the completion of irradiation, with a data acquisition duration of approximately 23.5 min.

F. Determination of cross sections and associated uncertainties

The formula for the activation cross section of ^{80}Kr(n, $2n$)^{79}Kr, as detailed in our earlier work [36, 37], is expressed as follows:

$$\sigma_x = \frac{[S\varepsilon I_\gamma \eta KMD]_{Nb}}{[S\varepsilon I_\gamma \eta KMD]_x} \cdot \frac{[\lambda AFC]_x}{[\lambda AFC]_{Nb}} \sigma_{Nb}, \tag{1}$$

where Nb and x represent the monitor and measured reactions, respectively. F is the total correction factor for the activity, which is given by

$$F = f_s \times f_c \times f_g \times f_\Omega, \tag{2}$$

where f_s, f_c, f_g, and f_Ω represent the correction factors for the self-absorption of the sample at a specific gamma energy, coincidence sum effect of cascade gamma rays within the studied nuclide, geometric configuration between the sample and detector, and solid angle subtended by the sample relative to the neutron source, respectively. The self-absorption of the eight characteristic rays emitted by ^{79}Kr in the sample was calculated using the weighted average formula provided earlier in our previous work [36].

$$f_s = 6\int_0^1 \frac{\mu r(1-r^2)}{1-\mathrm{e}^{-2\mu\sqrt{1-r^2}}}\mathrm{d}r, \tag{3}$$

The mass absorption coefficients (μ/ρ) of krypton and iron were interpolated from the values listed in Reference [38]. μ is the self-absorption absorption coefficient and ρ is the density. The coincidence summing correction factors for partial characteristic rays were corrected according to the method outlined in our earlier work [39]. The geometric correction for the sample was calculated

Table 1. Nuclear reactions measured on krypton and associated decay data (source: [24]).

Reaction	Abundance of target isotope (%)	Half-life of product	E-threshold /MeV	Mode of decay /%	$E\gamma$ /keV	$I\gamma$ (%)
^{80}Kr(n, $2n$)^{79m}Kr	99.928_{80}	50 s_3	11.799	IT(100)	130.01	100
^{80}Kr(n, $2n$)^{79g}Kr	99.928_{80}	35.4 d_7	11.668	EC(100)	**217.07**	**2.37_{13}**
					261.29	**12.7_4**
					299.53	**1.54_9**
					306.47	**2.60_{13}**
					388.97	**1.51_9**
					397.54	**9.3_4**
					606.09	**8.1_3**
					831.97	**1.26_7**
^{93}Nb(n, $2n$)^{92m}Nb	100	10.15 d_2	8.972	EC (100)	934.44	99.15_4

The black body is used in measurements. The uncertainty of ^{80}Kr abundance is estimated based on the product quality report.

using Eq. (4) [36]:

$$f_g = 3\int_0^1 \left(1+\frac{\sqrt{1-r^2}}{L}\right)^2 r\sqrt{1-r^2}\mathrm{d}r = 1+\frac{3}{2L}+\frac{3}{5L^2}, \quad (4)$$

The solid angle correction for the sample relative to the T-Ti target was calculated using Eq. (5) [36]:

$$f_\Omega = \frac{\frac{1}{2}(\Omega_1+\Omega_3)}{\Omega_2}, \quad (5)$$

In this experiment, the correction value was 1.0756.

III. UNCERTAINTY AND WEIGHTED AVERAGE

The uncertainties of the experimental cross sections corresponding to the eight characteristic rays were analyzed using the square root of the sum of squares method [40, 41]. According to Eq. (1), the main experimental quantities contributing to the uncertainties include the monitor reaction (0.55%−0.60%), detection efficiency (2.5%−3.0%), counting statistics (for lines 217.07 keV (1.70%−8.05%), 261.29 keV (0.38%−1.68%), 299.53 keV (2.55%−16.24%), 306.47 keV (1.57%−7.94%), 388.97 keV (2.41%−12.22%), 397.54 keV (0.52%−2.38%), 606.09 keV (0.58%−4.23%), 831.97 keV (4.24%−10.10%)), relative gamma ray intensity (0.04%−5.96%), half-life (0.20%−1.98%), sample weight (0.1%), timing (<0.1%), self-absorption of gamma ray (~0.5%), and isotopic abundance (0.08%).

A. Weighted average

Through analyzing the eight characteristic gamma rays emitted by the ^{79}Kr nucleus, the cross section of the ^{80}Kr(n, 2n) reaction can be expressed as follows: $\sigma_i \pm \Delta\sigma_i$, where i=1,..., 8. The uncertainties were normalized by taking the reciprocal of the squared uncertainty, and the weighted average cross section was calculated using the following formula [42]:

$$\sigma = \frac{\sum_{i=1}^{8}[\sigma_i/(\Delta\sigma_i)^2]}{\sum_{i=1}^{8}[1/(\Delta\sigma_i)^2]}, \quad (6)$$

B. Experimental standard deviation

The standard deviation of the experimental results was divided into Classes A and B. The experimental standard deviation, $\Delta\sigma_A$, was defined as follows [42]:

$$\Delta\sigma_A = \left[\frac{\sum_{i=1}^{n}[(\sigma_i-\sigma)^2/(\Delta\sigma_i)^2]}{(n-1)\sum_{i=1}^{n}[1/(\Delta\sigma_i)^2]}\right]^{1/2}, \quad (7)$$

A key challenge in experimental science is extracting the maximum information from a limited set of measurements. Specifically, Eq. (7), which calculates error $\Delta\sigma_A$ of the weighted mean, can yield unphysical results when applied to extremely small sample sizes. To address this problem, we introduce $\Delta\sigma_B$, which constrains the influence of individual errors on $\Delta\sigma$ [42]:

$$\Delta\sigma_B = \left[\sum_{i=1}^{n}\frac{1}{(\Delta\sigma_i)^2}\right]^{-1/2}, \quad (8)$$

However, Eq. (8) may also yield inaccurate results when two data points are significantly different but have relatively small error bars. In such cases, standard deviation $\Delta\sigma$ of weighted average σ can be calculated for a limited number of measurements using the following formula [42]:

$$\Delta\sigma = \max(\Delta\sigma_A, \Delta\sigma_B), \quad (9)$$

In this experiment, the uncertainty in the weighted average cross section ranged from 2.5% to 3.7%. The results are summarized in Table 2.

IV. MODEL AND SYSTEMATIC CALCULATIONS

A. Model calculations with TALYS-1.96

Calculations of cross sections based on nuclear models are crucial for evaluating reactor safety, as existing experimental data on the partial nuclear reaction cross sections caused by neutrons are limited or inconsistent [2, 44]. Nuclear reaction models are reliable methods for calculating energy and angle distributions, as well as activity yield cross sections, of reaction products [45]. These models account for direct interactions, thermal equilibrium, and precursor processes. Among the input parameters for cross section calculations, the energy level density is the most important [46]. The nuclear level density refers to the number of excited states per energy interval around a given excitation energy, *i.e.*, (dN/dE) per energy interval. In the low-energy region, the excited states are discrete; however, as the excitation energy increases, they transition to a continuous state. Therefore, a nuclear model is required to calculate energy density in the continuous energy region [45]. An accurate and reliable description of the excitation level of the nuclear states in

Table 2. Cross section values corresponding to different characteristic rays and their weighted average results.

Reaction	$E\gamma$ /keV	Cross sections (in mb) at various neutron energies (in MeV)				
		13.59±0.12	13.86±0.15	14.13±0.16	14.70±0.13	14.94±0.02
^{80}Kr(n, 2n)^{79}Kr	217.07	603±46	689±55	815±87	853±63	938±68
	261.29	673±37	776±43	813±46	952±52	960±52
	299.53	580±51	636±60	661±118	850±68	940±73
	306.47	642±46	728±53	802±83	867±61	960±66
	388.97	637±56	642±60	780±112	780±64	907±71
	397.54	687±43	803±50	849±56	969±60	1071±66
	606.09	704±42	859±51	911±65	1017±59	1129±65
	831.97	703±72	753±93	676±62	947±92	1122±93
Weighted average ± standard uncertainty		656±16	746±28	804±28	908±28	996±30
^{93}Nb(n, 2n)^{92m}Nb [43]	934.44	454.55±2.71	457.99±2.57	459.76±2.51	460.17±2.60	460.28±2.70

both low- and high-energy regions is necessary to verify the quality of the reaction model used for cross section calculations [47]. The TALYS code (version 1.96) [25] was employed to calculate partial and total cross sections, angle distributions, energy spectra, differential spectra, and recoil. It utilized a combination of microscopic and phenomenological nuclear cascade density models to generate nuclear cross sections. The theoretical excitation function for the ^{80}Kr(n, 2n)^{79}Kr reaction was computed across a neutron energy range from the reaction threshold up to 20 MeV using default parameters and adjustments only to the selected level density models. Further details on the cascade density parameters can be found in earlier reports [32].

B. Systematic calculations

Systematics, in addition to experimental measurements and theoretical calculations, serves as an effective approach for obtaining the cross section value for a certain reaction. The advantage of the systematics method is that it can predict the cross section values of reactions without experimental measurements based on the experimental cross section values of existing reactions. Many researchers [16−23] have used existing experimental data to develop various empirical and semi-empirical (systematic) formulas for calculating the cross section values at different neutron energies (see Table 3). Additionally, some researchers [1] have employed Bayesian neural network methods to predict the cross section values of (n, 2n) nuclear reactions. They selected three physical quantities, in addition to the proton and neutron numbers of the target nucleus, as the input parameters of the neural network: the incident neutron energy, odd-even effect, and theoretical value of the cross section. The systematic formulas collected indicated that the cross section is a function of the asymmetry parameter [(*N*-*Z*)/*A*], atomic mass number A, and incident neutron energy E_n. The cross section of the reaction can be expressed as follows:

$$\sigma_{n,2n} = f[E_n, A^{1/3}, (N-Z)/A], \tag{10}$$

The existing systematic formulas typically rely on statistical models designed for specific neutron energies, such as 14.5 MeV. The formation cross section in these formulas depends on mass number A of the target nucleus, whereas the Q-value effect is related to the number of protons and neutrons in the target nucleus.

V. RESULTS AND DISCUSSION

In this study, eight gamma rays with energies of 217.07 keV (I_γ=2.37%), 261.29 keV (I_γ=12.7%), 299.53 keV (I_γ=1.54%), 306.47 keV (I_γ=2.60%), 388.97 keV (I_γ=1.51%), 397.54 keV (I_γ=9.3%), 606.09 keV (I_γ=8.1%), and 831.97 keV (I_γ=1.26%) emitted in the decay of ^{79}Kr were used to measure the cross section of the ^{80}Kr(n, 2n)^{79}Kr reaction (E_{th}=11.668 MeV). The ^{93}Nb(n, 2n)^{92m}Nb reaction (E_{th}=8.972 MeV) was selected as the standard reaction to monitor the neutron flux. In previous measurements [14], the characteristic ray at 398 keV, along with the ^{27}Al(n, α)^{24}Na (E_{th}=3.249 MeV) and ^{56}Fe(n, p)^{56}Mn (E_{th}=2.966 MeV) monitor reactions, were used to determine the ^{80}Kr(n, 2n)^{79}Kr cross section. At a neutron energy of 14.4±0.3 MeV, the measured result was (810±60) mb, with an uncertainty of 7.4%. In the present study, we applied a weighted average method, which resulted in an uncertainty of less than 3.7% for the ^{80}Kr(n, 2n)^{79}Kr cross section. The measured cross sections and systematic calculation results are given in Table 4. The final correlation matrix for the ^{80}Kr(n, 2n)^{79}Kr reaction cross section is presented in Table 5. All experimental data, TALYS-1.96 theoretical calculation results, and systematic results are presented in Fig. 6. Additionally, the experimental results and evaluation curves of

Table 3. Comparison of (n, 2n) reaction cross section systematics.

Author	Formula, σ/mb	Mass region	E_n/MeV
Chatterjee *et al.* [16]	$\sigma_{n,2n} = 31.39(A^{1/3}+1)^2\exp(1.706(N-Z)/A)$	$45\leq A\leq 238$	14.5
Lu and Fink [17]	$\sigma_{n,2n} = 45.76(A^{1/3}+1)^2[1-7.372\exp(-32.21(N-Z)/A)]$	$28\leq Z\leq 82$	14.5
Bychkov *et al.* [18]	$\sigma_{n,2n} = 8.7(100+A)(1-0.88\exp(-7.95(N-Z)/A))$	$45\leq A\leq 238$	14.5
Konobeyev *et al.* [19]	$\sigma_{n,2n} = 53.066(A^{1/3}+1)^2\left\{1-\frac{43.5Q_{n'}^2-2Q_{n'}^3}{A^{1/3}S^3}\right\}$	$40\leq A\leq 209$	14.5
	$S = -11.068+270.15\left[\frac{N-Z+2.35}{A}\right]-753.93\left[\frac{N-Z+2.35}{A}\right]^2+\alpha_5\frac{1}{A^{3/4}}$		14.5
	$Q_{n'} = \begin{cases} 13.848-31.457\left[\frac{N-Z-0.5}{A}\right], & for\quad even-N \\ 9.846-19.558\left[\frac{N-Z-0.5}{A}\right], & for\quad odd-N \end{cases}$		14.5
	For even N, $\alpha_5 = 65.7$, for odd N, $\alpha_5 = 0$		14.5
Akash Hingu *et al.* [20]	$\sigma_{n,2n} = 1.344(A^{1/3}+1)^2\exp(40.53(N-Z)/A-116.5(N-Z)^2/A^2)$	$48\leq A\leq 238$ (even -A)	14.5
	$\sigma_{n,2n} = 4.39(A^{1/3}+1)^2\exp(27.77(N-Z)/A-82.26(N-Z)^2/A^2)$	$45\leq A\leq 209$ (odd -A)	14.5
Gehan Y. Mohamed *et al.* [21]	$\sigma_{n,2n} = A^{\frac{1}{3}}(a+cx^2+ex^4+gx^6+ix^8)/(1+bx^2+dx^4+fx^6+hx^8)$	$x=\exp[-((N-Z)/A)]$	13
	$\sigma_{n,2n} = A^{\frac{1}{3}}(a+cx^2+ex^4+gx^6+ix^8+kx^{10})/(1+bx^2+dx^4+fx^6+hx^8+jx^{10})$		14
	$\sigma_{n,2n} = A^{\frac{1}{3}}(a+cx+ex^2+gx^3)/(1+bx+dx^2+fx^3)$		15
Habbani *et al.* [22]	$\sigma_{n,2n} = 23.53(A^{1/3}+1)^2\exp(3.50(N-Z)/A)$	$45\leq A\leq 209$ (odd -A)	14.5
	$\sigma_{n,2n} = 20.82(A^{1/3}+1)^2\exp(3.76(N-Z+1)/A)$	$48\leq A\leq 238$ (even -A)	14.5
Luo *et al.* [23]	$\sigma_{n,2n} = 0.0226(1+A^{1/3})^2\exp(133.86(N-Z)/A-779.47(N-Z)^2/A^2+1500.51(N-Z)^3/A^3)$	$23\leq A\leq 209$	14.5

Table 4. Measured cross sections and systematic results of the ^{80}Kr(n, 2n)^{79}Kr reaction at corresponding neutron energies.

Refs.	E_n /MeV	Cross sections /mb
Present experimental results	13.59±0.12	656±16
	13.86±0.15	746±28
	14.13±0.16	804±28
	14.70±0.13	908±28
	14.94±0.02	996±30
Kondaiah *et al.* [14]	14.4±0.3	810±60
Systematic result		
Chatterjee *et al.* [16]	14.5	1049
Lu and Fink [17]	14.5	910
Bychkov *et al.* [18]	14.5	944
Konobeyev *et al.* [19]	14.5	1149
Akash Hingu *et al.* [20]	14.5	680
Gehan Y. Mohamed *et al.* [21]	131415	53515512081
Habbani *et al.* [22]	14.5	896
Luo *et al.* [23]	14.5	766

databases ENDF/B-VIII.0 [26] (BROND-3.1 [27]), JEFF-3.3 [28], JENDL-5 [29], and TENDL-2023 [30] are shown in Fig. 7. To compare the experimental results with the theoretical (evaluated) values, we calculated the $\chi^2 = \frac{1}{N}\sum_{i=1}^{N}[(\sigma_i^{\rm calc}-\sigma_i^{\rm exp})/(k\Delta\sigma_i^{\rm exp})]^2$ values [32]. The results are provided in Tables 6 and 7. Figure 6 clearly shows that, in the energy range of 13−15 MeV, our experimental results are consistent with the systematic results of Lu and Fink [17], Bychkov *et al.* [18], and Habbani *et al.* [22], as well as the TALYS-1.96 theoretical results using ldmodel 5 within the uncertainty range (see Table 6). However, our results are higher than the calculations of TALYS-1.96 corresponding to ldmodels 3, 4, and 6. In particular, the theoretical results of ldmodel 3 have a significant deviation from those of the other ldmodels. This indicates that the generalized superfluid model (ldmodel 3) is insufficient to accurately describe the reaction ^{80}Kr(n, 2n)^{79}Kr. Fig. 7 shows that our measurement results in the neutron energy range of 13−14.7

Table 5. Results of the ^{80}Kr(n, 2n)^{79}Kr reaction, encompassing experimental cross sections, overall uncertainties, and correlation matrices.

Neutron energy E_n /MeV	Cross section σ_x /mb	$\Delta\sigma_x$ (%)	Correlation matrix				
13.59±0.12	656±16	2.5	1.0000				
13.86±0.15	746±28	3.7	0.3912	1.0000			
14.13±0.16	804±28	3.5	0.4815	0.4751	1.0000		
14.70±0.13	908±28	3.1	0.3916	0.3847	0.4714	1.0000	
14.94±0.02	996±30	3.1	0.3967	0.3896	0.4770	0.3907	1.0000

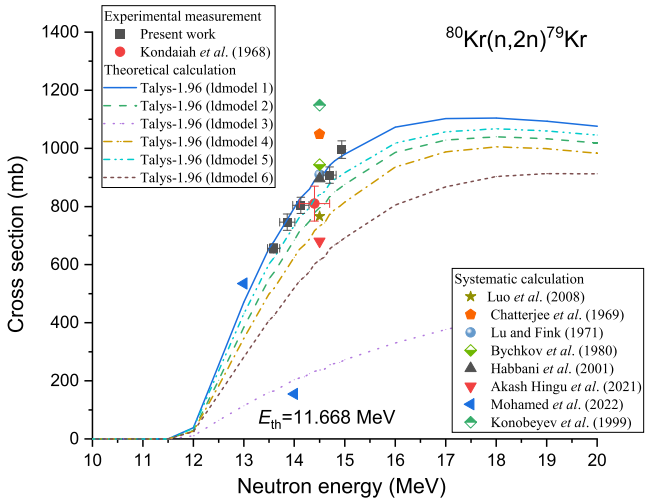

Fig. 6. (color online) Theoretical excitation function of ^{80}Kr(n, $2n$)^{79}Kr reaction, experimental data, and systematic results.

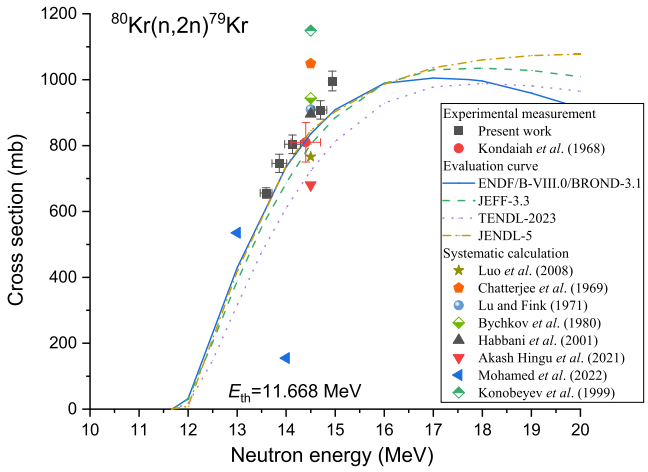

Fig. 7. (color online) Experimental values and evaluation curves of ^{80}Kr(n, $2n$)^{79}Kr reaction.

MeV are also consistent with the evaluation curves of ENDF/B-VIII.0 and BROND-3.1 (see Table 7). However, at the energy point of 14.94±0.02 MeV, our results are slightly higher than the evaluation curves [26−30]. At 14.4±0.3 MeV, our results agree only with the values in Reference [14]. At 14.5 MeV, the systematic results are distributed between 680 and 1149 mb. Note that three systematic formulas in Reference [21] provide calculations at 13, 14, and 15 MeV, yielding values of 535, 155, and 1,2081 mb, respectively. The results at the energy points of 14 and 15 MeV exhibit significant anomalies. The possible reason is that the empirical formula provided in Reference [21] contains inaccuracies, as it fails to reproduce their own results. The data point 1,2081 mb was excluded from Figs. 6 and 7 owing to its significantly larger magnitude than the other values.

Table 6. Comparison between the current measured cross section and the TALYS-1.96 theoretical value corresponding for each level density model (covering factor k=2, confidence P=95%).

Reaction	χ^2 (k=2, P=95%)					
	ldmodel 1	ldmodel 2	ldmodel 3	ldmodel 4	ldmodel 5	ldmodel 6
^{80}Kr(n, $2n$)^{79}Kr	0.984	3.769	146.031	9.940	**0.963**	28.567

The minimum value in each row is indicated in bold.

Table 7. Comparison between the cross section measured and evaluation value (covering factor k=2, confidence P=95%). ENDF/B-VIII.0 is the same as BROND-3.1.

Reaction	χ^2 (k=2, P=95%)			
	ENDF/B-VIII.0	JEFF-3.3	JENDL-5	TENDL-2023
^{80}Kr(n, $2n$)^{79}Kr	**1.342**	3.453	1.397	11.854

The minimum value in each row is indicated in bold.

VI. CONCLUSION

The activation cross sections for the ^{80}Kr(n, $2n$)^{79}Kr reaction were measured at neutron energies of 13.59±0.12, 13.86±0.15, 14.13±0.16, 14.70±0.13, and 14.94±0.02 MeV using updated decay data. The activity of the generated nuclei was assessed by analyzing eight characteristic gamma rays emitted by ^{79}Kr. The precision of the measurement was significantly improved through the application of a weighted averaging method. Compared with previous studies, the current cross section data covered a broader energy range and exhibited lower uncertainties. The theoretical cross sections for the ^{80}Kr(n, $2n$)^{79}Kr reaction were computed using the TALYS-1.96 code with various level density models. Our experimental results were compared with earlier experimental values, theoretical predictions from different models, evaluated curves, and results derived from systematic formulas. The nuclear model calculations using the TALYS code indicated that the microscopic level densities (Skyrme force) composed from Hilaire's combinatorial tables [48] (ldmodel 5) were the most suitable for describing the cross section of the ^{80}Kr(n, $2n$)^{79}Kr reaction. The data obtained in this study are crucial for improving nuclear data libraries, validating nuclear reaction models, and supporting practical applications. Moreover, the high-precision cross section data provide strong support for parameter fitting in systematic formulas for (n, $2n$) reactions and training neural networks.

ACKNOWLEDGEMENTS

We would like to thank the Intense Neutron Generator group at Chinese Academy of Engineering Physics for performing the irradiations.

References

[1] W. Li, L. Liu, Z. Niu *et al*., Phys. Rev. C **109**, 044616 (2024)
[2] K. Blaum and M. J. G. Borge, Eur. Phys. A **60**, 94 (2024)
[3] S. M. Qaim, Nucl. Med. Biol. **44**, 31 (2017)
[4] L. He, J. Luo, and L. Jiang, Chin. Phys. C **47**, 034001 (2023)
[5] J. Luo, L. Jiang, J. Liang *et al*., Chin. Phys. C **46**, 044001 (2022)
[6] IAEA experimental nuclear reaction data (EXFOR) Brookhaven National Laboratory, 2022. National nuclear data center https://www-nds.iaea.org/exfor/exfor.htm
[7] A. Gandhi, A. Sharma, R. Pachuau *et al*., Eur. Phys. J. Plus **136**, 819 (2021)
[8] J. Luo, L. Jiang, and J. Liang, Eur. Phys. A **60**, 2 (2024)
[9] J. Luo, L. Jiang, F. Tuo *et al*., Phys. Scr. **99**, 045034 (2024)
[10] J. Luo, F. Tuo, and X. Kong, Phys. Rev. C **79**, 057603 (2009)
[11] Akash Hingu *et al*., Chin. Phys. C **48**, 024001 (2024)
[12] Vibhuti Vashi *et al*., Phys. Rev. C **105**, 044613 (2022)
[13] M. Bhike, E. Rubino, M. E. Gooden *et al*., Phys. Rev. C **92**, 014624 (2015)
[14] E. Kondaiah, N. Ranakumar, and R. W. Fink, Nucl. Phys. A **120**, 337 (1968)
[15] J. Zeng, C. Zhu, Y. Gong *et al*., Nucl. Phys. A **1030**, 122569 (2023)
[16] S. Chatterjee and A. Chatterjee, Nucl. Phys. A **125**, 593 (1969)
[17] W.-d. Lu and R. W. Fink, Phys. Rev. C **4**, 1173 (1971)
[18] V. M. Bychkov, V. N. Manokhin, A. B. Pashchenko *et al*., INDC(CCP)-146, NDS, IAEA, 1980
[19] A. Yu. Konobeyev and Y. A. Korovin, Nuovo Cimento A **112**, 1001 (1999)
[20] A. Hingu, S. Parashari, S. K. Singh *et al*., Radiat. Phys. Chem. **188**, 109634 (2021)
[21] G. Y. Mohamed, M. Al-abyad, and A. Azzam, Appl. Radiat. Isot. **187**, 110341 (2022)
[22] F. I. Habbani and Khalda T. Osman, Appl. Radia. Isoto. **54**, 283 (2001)
[23] J. Luo, F. Tuo, F. Zhou *et al*., Nucl. Instrum. Meth. B **266**, 4862 (2008)
[24] B. Singh, Nucl. Data Sheets **135**, 193 (2016)
[25] A. J. Koning, S. Hilaire, and M. Duijvestijn, TALYS-1.96, *A nuclear reaction program*, NRG-1755 ZG Petten, Netherlands, 2021 http://www.talys.eu
[26] D. A. Brown *et al*., Nucl. Data Sheets **148**, 1 (2018)
[27] A. I. Blokhin *et al*., Vopr. At. Nauki Tekh. Ser. Yad. Konstanty **2**, 62 (2016)
[28] A. J. M. Plompen *et al*., Eur. Phys. A **56** , 181 (2020)
[29] O. Iwamoto *et al*., J. Nucl. Sci. Technol. **60** , 1 (2023)
[30] A. J. Koning, D. Rochman, J. -Ch. Sublet *et al*., Nucl. Data Sheets **155**, 1 (2019)
[31] Evaluated Nuclear Structure Data File (ENSDF), (Last updated 2024-11-07) https://www.nndc.bnl.gov/nudat3/
[32] J. Luo, L. He, L. Zhou *et al*., Eur. Phys. A **61**, 30 (2025)
[33] V. E. Lewis and K. J. Zieba, Nucl. Instrum. Meth. **174**, 141 (1980)
[34] J. Luo, L. Du, J. Zhao *et al*., Nucl. Instrum. Meth. B **298**, 61 (2013)
[35] GammaVision®-32, *Gamma-Ray Spectrum Analysis and MCA Emulator*, Software User's Manual, Software Version 5.3.
[36] J. Luo, J. Liang, L. Jiang *et al*., Eur. Phys. A **58**, 142 (2022)
[37] J. Luo, J. Liang, L. Jiang *et al*., Nucl. Sci. Tech. **34**, 4 (2023)
[38] J. H. Hubbell and S. M. Seltzer, *Tables of x-ray mass attenuation coefficients and mass energy-absorption coefficients from 1 keV to 20 MeV for elements Z = 1 to 92 and 48 additional substances of dosimetric interest* (1995) http://physics.nist.gov/PhysRefData/XrayMassCoef/tab3.html
[39] F. Zhou, Y. Zhang, J. Luo *et al*., HEP & NP **31**, 487 (2007) (in Chinese)
[40] N. Otuka, B. Lalremruata, M. U. Khandaker *et al*., Radiat. Phys. Chem. **140**, 502 (2017)
[41] M. Choudhary *et al*., Chin. Phys. C **48**, 094104 (2024)
[42] J. Luo and L. Jiang, Eur. Phys. A **55**, 27 (2019)
[43] IRDFF-II (International Reactor Dosimetry and Fusion File), 2020 https://www-nds.iaea.org/IRDFF/
[44] S. Hoblit, Y. -S. Cho, M. Herman *et al*., Nucl. Data Sheets **112**, 3075 (2011)
[45] G. Schnabel, *Fitting and analysis technique for inconsistent nuclear data*, 2017 − International Conference on Mathematics & Computational Methods Applied to Nuclear Science & Engineering, Jeju, Korea, April 16−20, 2017, on USB (2017)
[46] A. Koning, S. Hilaire, and S. Goriely, Eur. Phys. A **59**, 131 (2023)
[47] S. Sudár and S. M. Qaim, Nucl. Phys. A **979**, 113 (2018)
[48] RIPL-2 Reference Input Parameter Library, IAEA, A-1400Vienna, IAEA-NDS http://www-nds.iaea.org/RIPL-2/